135 YEARS OF NAVAL ENGINEERS JOURNAL

Summer 2023 | Vol. 135 | No. 2

# NEJ

## Dialing for Dollars

Creating Affordability in Defense Through Enterprise Design **71**

## Special Section—Intelligent Ships Symposium 2023 **45**



www.navalengineers.org

NEJ

## DEPARTMENTS



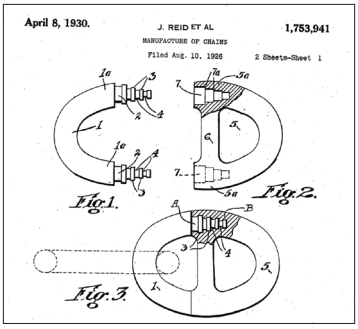






## FEATURES & NEWS



## Special Section — Intelligent Ships Symposium 2023

# Application of Magnetic Bearings to the Navy HESC Chiller Compressor: Vibration and Shock Modelling and Testing

Larry Hawkins[1], Rasish Khatri[1], Koman Nambiar[2], Kevin Wiley[3], Alberto Tecce[3], Haley Galloway[3]

## Abstract

**Active magnetic bearings (AMBs) have recently been applied in the new Navy HESC chiller compressor due to advantages over conventional hydrodynamic bearings, including high surface speed, oil free operation in refrigerants, low losses, efficient low speed operation, and built-in diagnostic and monitoring features. The compressor was designed and tested for the MIL-STD-167-1A external vibration requirement and the MIL-S-901D shock standard. A linear forced response analysis with base motion input was used to predict chiller rotor displacements and magnetic bearing loads due to the MIL-STD-167-1A excitation. The predictions were used to guide AMB sizing and control algorithm design. A transient, nonlinear model was developed to simulate the floating platform shock testing. The simulation includes rotor and housing structural models, the magnetic bearing control and saturation features, backup bearings with resilient mounts and associated clearances. As the shock events are expected to be rare and substantially exceed the operating loads, the system is designed such that shock is absorbed by a backup (touchdown) bearing system. The simulation results were used to evaluate backup bearing loads and the backup bearing shock mount design. Comparisons of predictions and measured responses from both test series are shown here to demonstrate good agreement. The HES-C chiller system is now in serial production. As of the date of publication, over 15 complete HESC chiller systems have been successfully commissioned.**

## Introduction

Shipboard cooling requirements have steadily increased due to steadily increasing use of communications equipment and high-energy directed energy equipment. This has necessitated the United States Navy to find a cooling solution that improves cooling capacity within the same space as legacy cooling systems and improves cooling capacity for next-generation ships. As with other high-capital cost equipment used in the defense sector, the cooling solution must have high-reliability and relatively low lifecycle cost. As a result, Naval Sea Systems Command and Johnson Controls Naval Systems have developed the High Efficiency Super-Capacity (HESC) water chiller (Figure 1), with Calnetix Technologies providing the motor, bearings, and important motor drive components. Key aspects of the development of the magnetic bearing system for this application will be discussed further. This chiller has a cooling capacity of 375 tons, 175 tons more than the legacy 200 ton R134a chiller installed on DDG Flight IIA and LPD17 Class platforms and can deliver this cooling capacity while providing 42 deg. F chilled water.

The chiller is intended to be installed on the Arleigh Burke class destroyer (DDG), San Antonio class landing platform/dock (LPD), and the Constellation class frigate (FFG). The DDG Flight III ships require at least 50% more cooling capacity than DDG Flight IIA ships, making the HESC a logical choice. LPDs have chosen to go with the HESC as it helps to meet the objectives of: (1) reducing ship acquisition cost, (2) increasing cooling density to provide more cooling in the same space, and (3) improving life cycle cost. The first Constellation class frigate (FFG-62) will enter into service in 2026, and each ship of this class is expected to have HESC chillers installed as they were a logical choice for cooling capacity, space, and fleet commonality reasons.

[1] Calnetix Technologies
[2] Johnson Controls Naval Systems
[3] Naval Sea Systems Command

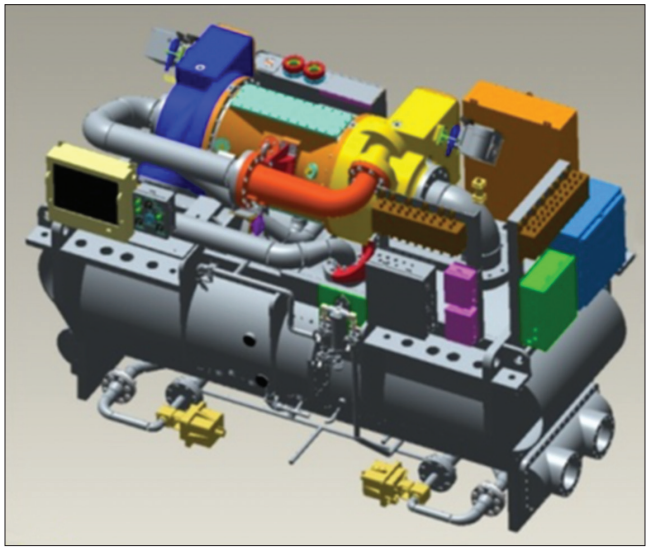

**FIGURE 1.** HESC water chiller

| Frequency Hz | Max 0 — pk Displacement (inch) | Acceleration at highest frequency | |
|---|---|---|---|
| | | Max in/sec^2 | Max g's |
| 4 to 10 | 0.150 | 592 | 1.53 |
| 11 to 15 | 0.036 | 320 | 0.83 |
| 16 to 25 | 0.024 | 592 | 1.53 |

**TABLE 1.** Magnetic Bearing Vibration Test per modified MIL-STD-167-1A

| Shot | Standoff, ft (m) (horz. distance from barge) | Shot direction | Chiller/Comp Operating Condition |
|---|---|---|---|
| 1 | 40 (12.2) | Fore-aft | Normal Operation |
| 2 | 30 (9.1) | Athwartship | Normal Operation |
| 3 | 25 (7.6) | Athwartship | Standby (de-levitated) |
| 4 | 20 (6.1) | Athwartship | Normal Operation |

**TABLE 2.** Shock Test Sequence

As risk-mitigation to operational vibration and shock loads, the system was designed to meet modified Type I vibration requirements in accordance with MIL-STD-167-1A[1] and shock testing requirements per MIL-S-901D.[2] The compressor was required to meet both vibration and shock requirements as a stand-alone unit and later also to meet both vibration and shock requirements as part of the operating chiller system. This paper summarizes these two requirements, shows how the system was modelled to simulate each of these tests, and shows how test data compared to the simulations.

The Navy's MIL-STD-167 vibration testing is formulated to assess two categories of vibration failure: (1) insufficient stiffness or clearance in the design, and (2) mechanical fatigue caused by long-duration cyclic loading. To meet these criteria, the Johnson Controls Navy Systems prototype compressor was first tested to the vibration levels of Table 1 as standalone unit during the development phase of the program. The operating chiller/compressor system was later tested to slightly lower levels and frequencies pursuant to the requirements of the intended ship platforms. Additionally, for both test series, the system was endurance tested with "unrealistically" large base excitations designed to mimic the same fatigue experienced with lower "realistic" vibration levels over several years.

The acceptance criteria for the vibration test includes:

1. The magnetic bearings must maintain stable rotor levitation throughout each test.
2. Magnetic Bearing Controller (MBC) ambient temperature must not exceed 60°C (140°F) throughout each test.
3. MBC amplifier temperatures must not exceed 95°C (203°F) throughout each test.
4. The HES-C compressor must maintain structural and electrical integrity throughout each test.

The size and weight of the new chiller necessitates shock testing be performed using the Heavy Weight or Floating Shock Platform (FSP). For this test, the HESC Chiller was installed on a FSP and subjected to a series of four shock impacts from high-explosive charges positioned 24-feet under the water. As dictated by the standard, one blast was 40-feet from the front of the floating platform and the other three blasts were 30-feet, 25-feet and 20-feet respectively from the side of the platform. The chiller was operating during three blasts and in standby mode for one blast, as summarized in Table 2.

The acceptance criteria for the shock test includes:

1. The backup bearing system of the compressor must absorb the shock impacts without mechanical failure
2. The magnetic bearings must be able to recover levitation of the rotor after the vibration response of the chiller caused by the explosive charge has decayed
3. The motor must be able to perform to full capacity without any issues

## Magnetic Bearing Design and Control

Magnetic bearings levitate a rotating shaft by applying forces on the rotor in five axes. The magnetic bearing must be able to apply translation forces to the rotor in three orthogonal directions and must be able to provide moment forces about the lateral (radial) axes. To accomplish this, a typical

**FIGURE 2.** General assembly of Radial Brg 1 (non-thrust end), sensor and touchdown bearing.[2]

magnetic bearing arrangement uses a four-quadrant/2-axis radial bearing on one end of the machine, another radial magnetic bearing on the opposite end of the machine, and a thrust magnetic bearing. Generally speaking, industrial magnetic bearings are usually *active*, meaning the force generated by the magnetic bearing is actively controlled by means of an electromagnet, position sensors, a control compensator, and power amplifiers all connected in a feedback control loop.

Electromagnets produce a force proportional to the square of the air gap flux which is in turn directly proportional to coil current. In all industrial magnetic bearings, the force/current relationship is linearized by imposing a bias flux. The bias flux can be generated by using electromagnets (EM) or by using permanent magnets (PM). The HESC motor utilizes homopolar, PM-biased radial magnetic bearings and an EM-biased axial magnetic bearing. PM-bias magnetic bearings have higher efficiency, virtually no heat generation, higher reliability, lower complexity, and higher force bandwidth relative to EM-bias magnetic bearings. EM-bias bearings are generally less capital-intensive (lower up-front cost) and the bias can be de-activated. The two radial bearings in this machine each have design load capacity of 3,122 N (700 lbf) and actuator negative stiffness of 6,150 N/mm (35,000 lbf/in). In this document, the non-thrust end radial bearing, shown in Figure 2, is often referred to as Brg 1, and the thrust end radial bearing is often referred to as Brg 2. The axial bearing has design load capacity of 6,244 N (1400 lbf) and a negative stiffness of 7,125 N/mm (40,000 lbf /in).

In order to control the force from each magnetic bearing, an appropriate control compensator was designed for each of the five magnetic bearing axes. Figure 3 summarizes the key elements of the single-input-single-output (SISO) magnetic bearing control loop. The rotor motion is detected by position sensors in all five AMB axes. The sensor signal is processed by a digital signal processor (DSP) and compared with a reference setpoint (usually the center of the touchdown bearings). A compensator calculates the net force required to adjust the rotor position in order to minimize the error between the reference setpoint and the sensed rotor position. Then, a command is sent to the digital power amplifier which adjusts a PWM duty-cycle to apply a voltage across the magnetic bearing electromagnets. This results in a change in current flowing through the electromagnets, which produces a force applied to the rotor.

A final key element to any magnetic bearing system is a touchdown bearing. A touchdown bearing, also called a back-up bearing, is a wear component used to catch the rotor during unsual overload or power loss events ("touchdown events"), to protect critical components in the machine. The HESC chiller motor uses greased angular contact ball bearings in a face-to-face duplex pair arrangement. Because the stiffness of the ball bearing pair is relatively high, the bearings are installed into a resilient mount, which serves to soften the landing of the rotor during a touchdown event and sets the whirl frequency of the spinning rotor on the touchdown bearings to a low value (typically below 200 Hz). The radial end touchdown bearing is shown on the right side of Figure 2.

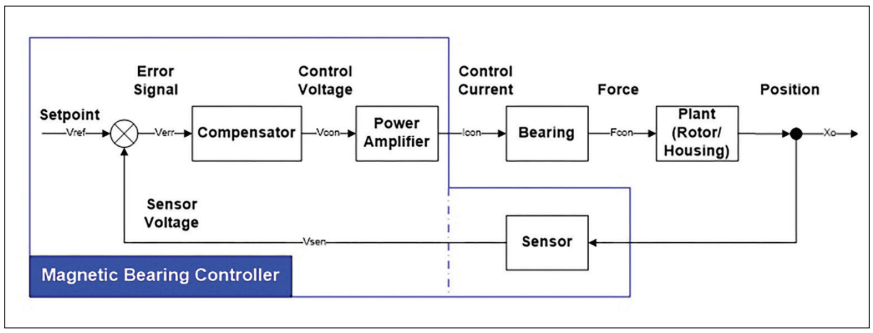


**FIGURE 3.** Magnetic bearing control loop

## System Modelling

A system model was created to aid the development of an initial stabilizing magnetic bearing compensator as well as to analyze the behavior of the compressor on the shaker table. This model, shown in Figure 4, includes a rotordynamic structural model, housing structural model and a model of the five axis magnetic bearing system. The rotor and housing models are created per industry standard practice with Timoshenko beam elements and mass lumped at the nodes and impeller rigid body mass, polar and transverse inertia lumped at the impeller centers-of-gravity. The housing is relatively simple, but provides a good representation of the mass distribution and appropriate nodes for connecting the housing supports (and shaker forces) and magnetic bearing connecting elements (sensors, actuator, and backup bearings). For the vibration analysis, the housing is connected to ground with discrete springs and dampers at the support locations.

The rotordynamic equation of motion for the compressor, which is in general a coupled, flexible rotor/housing system, is:

$$\begin{bmatrix} \mathbf{M}_R & 0 \\ 0 & \mathbf{M}_C \end{bmatrix} \begin{Bmatrix} \ddot{\mathbf{q}}_R \\ \ddot{\mathbf{q}}_C \end{Bmatrix} + \begin{bmatrix} \mathbf{D}_R + \mathbf{G}_R & 0 \\ 0 & \mathbf{D}_C \end{bmatrix} \begin{Bmatrix} \dot{\mathbf{q}}_R \\ \dot{\mathbf{q}}_C \end{Bmatrix} + \begin{bmatrix} \mathbf{K}_R + \mathbf{K}_{B1} & \mathbf{K}_{B2} \\ \mathbf{K}_{B3} & \mathbf{K}_C + \mathbf{K}_{B4} \end{bmatrix} \begin{Bmatrix} \mathbf{q}_R \\ \mathbf{q}_C \end{Bmatrix} = \begin{Bmatrix} \mathbf{f}_{mb,R} \\ \mathbf{f}_{mb,C} \end{Bmatrix} + \begin{Bmatrix} \mathbf{f}_{ext,R} \\ \mathbf{f}_{ext,C} \end{Bmatrix} \quad (1)$$

Or equivalently

$$\mathbf{M}\ddot{\mathbf{q}} + \mathbf{D}\dot{\mathbf{q}} + \mathbf{K}\mathbf{q} = \mathbf{f}_{mb} + \mathbf{f}_{ext} \quad (2)$$

Where the subscripts **R** and **C** represent rotor and casing (housing) elements respectively, **M**, **D**, and **K** matrices represent mass, damping and stiffness matrices, **G** is the rotor gyroscopic matrix containing skew symmetric entries of polar inertia times spin speed, and **q** is the physical displacement vector. Control forces from the magnetic bearing are introduced (coupled) in the force vector, $\mathbf{f}_{mb}$, and the external force vector, $\mathbf{f}_{ext}$, contains other external forces such as unbalance forces on the rotor, shaking forces from the vibration table into the housing model. For machines with conventional bearings or seals, the associated rotordynamic coefficients can be entered directly into the **M**, **D**, and **K** matrices.

A typical magnetic bearing transfer function is shown in Figure 5. This is a force/displacement transfer function such that the gain is the ratio of the applied actuator force (in dB lbf/inch) over the rotor/housing relative displacement at the postion sensor location. The phase plot shows the phase lead of the applied force to the sensed displacement. Phase lead between 0 and +90 degrees at a given frequency indicate positive stiffness and positive damping at that frequency. For linear system analysis, the magnetic bearing transfer function equations for each control axis are converted to state space form and coupled to the rotordynamic model (also converted to state space form) at the sensor and actutor degrees-of-freedom. The combined model in standard form is in Equation 3, where the external force vector, fext can be used to apply rotor unbalance or inject shaking forces.

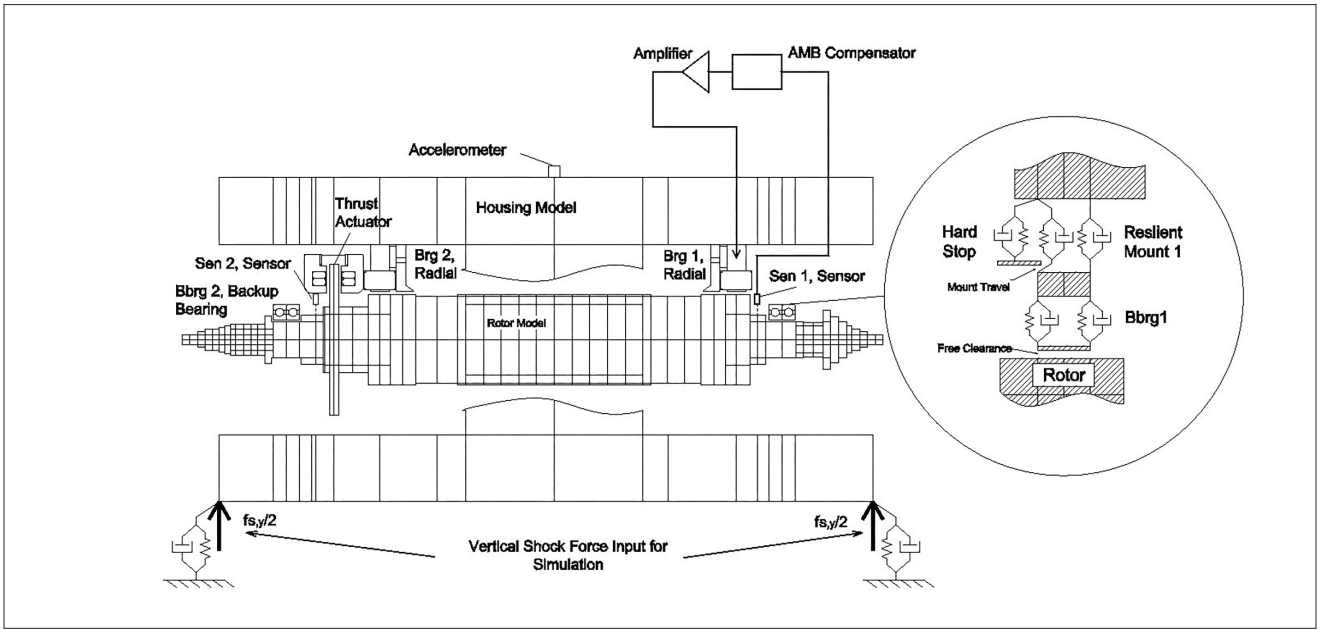


**FIGURE 4.** Compressor model with rotor, housing, magnetic bearings and backup (touchdown) bearings.[5]

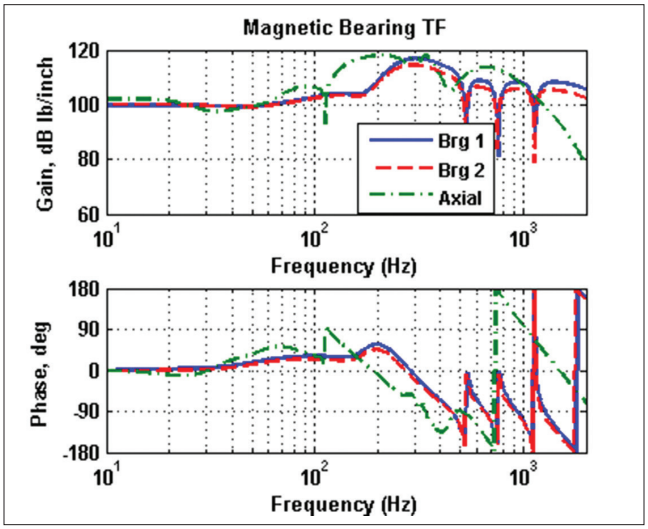


**FIGURE 5.** Typical magnetic bearing transfer function.[3]


**FIGURE 6.** Compressor on shaker table for stand-alone tests[3]

$$\dot{\mathbf{x}}_{sys} = \mathbf{A}_{sys}\mathbf{x}_{sys} + \mathbf{B}_{sys,ext}\,\mathbf{f}_{ext} \quad (3)$$

$$\mathbf{y} = \mathbf{C}_{sys}\mathbf{x}_{sys} \quad (4)$$

To perform the required frequency response analysis to model the compressor system on the shaker table, the Laplace transform is taken, yielding:

$$(s\mathbf{I} - \mathbf{A}_{sys})\mathbf{X}_{sys}(s) = \mathbf{B}_{sys,ext}\,\mathbf{F}_{ext}(s) \quad (5)$$

Often the excitation forces are known, so at each analysis frequency, the known excitation forces are loaded into the force vector and Eq. (5) is solved for the states **X**sys. Rotor and housing displacements and magnetic bearing control forces can be retrieved from **X**sys using the output description in Eq. (4). In this case, the housing base motion is prescribed by Table 1 so the approach had to be altered. One option is to intially run the frequency response analysis with a constant amplitude force vector.

The predicted base displacements versus frequency can then be used to scale the force vector for a subsequent analysis run to get the desired base amplitude versus frequency. This is the approach used here.

The system model and subsequent analysis was developed in more detail by Hawkins.[3] Additional detail on magnetic bearing modelling can be found in the text by Schweitzer and Maslen.[4]

## MIL-STD-167 Analysis & Testing

As discussed above, the compressor was to be tested to the modified MIL requirements from Table 1. When tested, the compressor was placed on a shaker table, Figure 6, and the excitation imposed one frequency at a time starting at the lowest frequency and stepping to the highest frequency in 1 Hz increments. There are three frequency ranges with each having a different base motion amplitude. The highest accelerations and therefore highest bearing loads occur at the highest frequency in each range. The vibration testing and modelling summarized here was previously covered in more detail by Hawkins.[3]

The system model described in the previous section was used pre-test to ensure that the developed magnetic bearing control compensator (magnetic bearing transfer function) was stiff enough to prevent backup bearing contact during the worst case excitation. If there is no other driving requirement, such as this external vibration requirement, a standard magnetic bearing compensator is relatively soft in the frequency range of 4 – 25 Hz.

The results of the testing and analysis for vertical shaking are shown in Figures 7 to 10. Data collected during the shaker tests include: shaker table acceleration in the excitation direction, position sensor displacement and commanded current for all five magnetic bearing control axes, actuator temperatures, and MBC amplifier and ambient temperatures. The shaker table acceleration data was recorded manually from the vibration monitors once for each frequency. Position sensor displacement and current command data were collected at 5 kHz by the magnetic bearing GUI (Graphical User Interface). For each frequency, average amplitude at the excitation frequency over the five minute excitation period was used to represent the sensor displacement and current at each frequency. Measured actuator control forces are calculated from the measured current command data by multiplying by the known amplifier

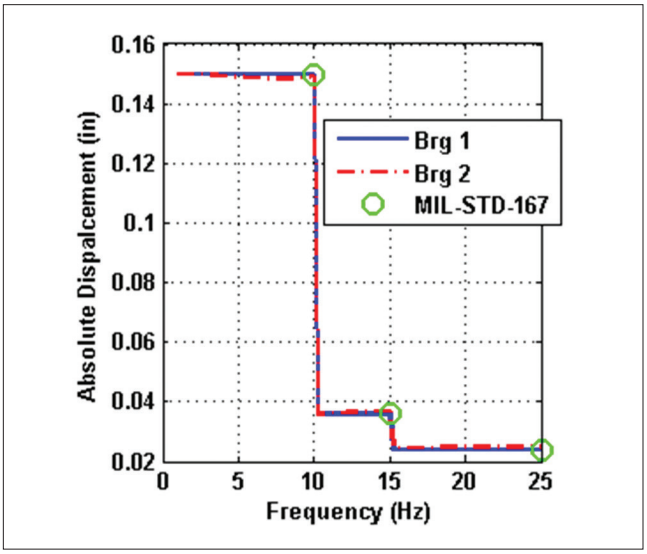


**FIGURE 7.** Measured housing vibration during shaker table testing.[3]

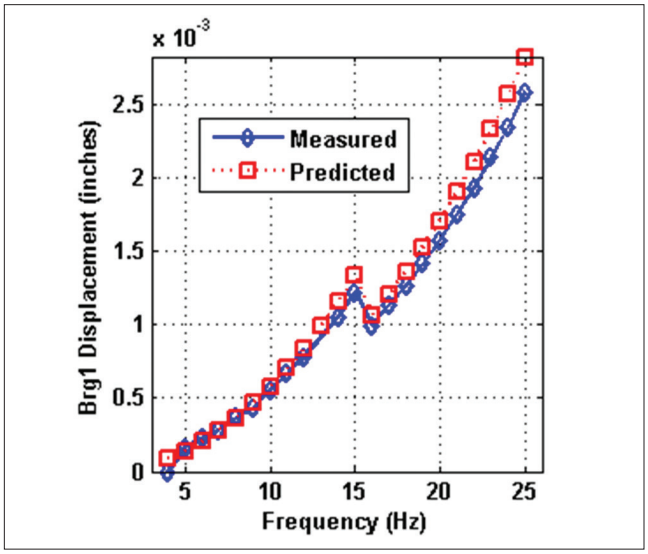


**FIGURE 8.** Measured and predicted rel. rotor/housing displacement at Brg 1 position sensors using measured housing vibration as input.[3]

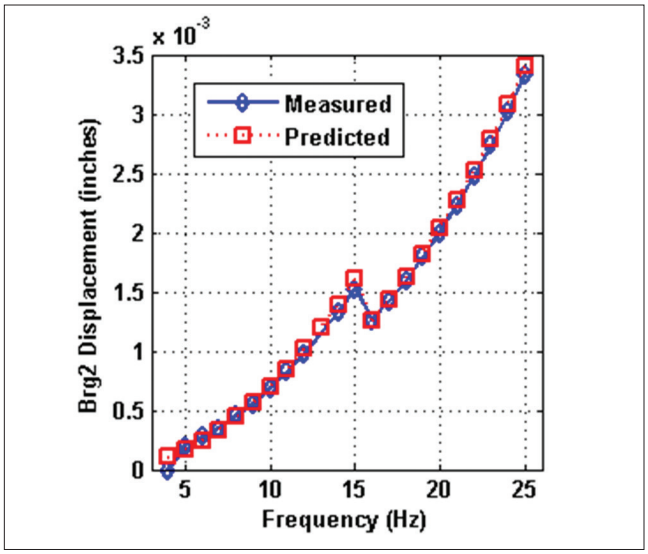


**FIGURE 9.** Measured and predicted rel rotor/housing displacement at Brg 2 position sensors using measured housing vibration as input.[3]

transfer function and by the actuator transfer function. For the radial measurements shown, the bandwidth of the actuator is well above the maximum excitation frequency so the transfer function is essentially constant and equal to the actuator gain in lbf/amp or N/amp. The Brg 1 and Brg 2 load measurements represent the vector sum of the X and Y axis loads calculated from X and Y axis current command data as just described.

Figure 7 shows the target base motion versus frequency per Table 1 along with measured base motion versus frequency for the two ends of the housing. Clearly the response in the 4 – 10 Hz range is well below the requirement. The displacement was limited by the capability of the shaker table equipment at the independent test lab. The shortcoming was known and approved pre-test by the Navy as the largest load and largest demand on the MBC are at the highest excitation frequency (25 Hz).

Another shortcoming of the test data is the difference in measured displacement at the two ends of the machine. Two possible sources of the error were identified: 1) the center-of-gravity of the compressor was not in line with the force axis of the shaker table, and 2) incorrect calibration of the housing accelerometers used to quantify base motion. The difference in the two measurments is approximately 0.003 inch (± 0.0015 inch) in the frequency range between 15 and 25 Hz or about ±6%. For the predicted results shown below, the measured housing motions of Figure 7 were taken at face value and used to create the forcing function for the analysis.

Predicted and measured frequency response results are shown in Figures 8-10. The predictions are calculated using the system model described in the previous section with the measured housing vibration from Figure 7 as the driver. Predicted and measured relative displacement at the Brg 1 and Brg 2 sensors are shown in Figures 8 and 9, respectively. Since the vibration was vertical and between the two poles of the bearing, the measured displacement is the vector sum of the X and Y position sensor measurements and predictions. The maximum measured displacement, 0.0034 inch, occurs at Brg 2 at 25 Hz, and is well within the allowable displacement.

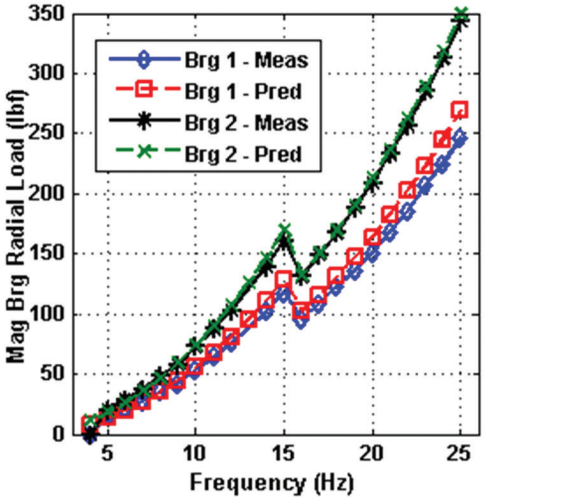


**FIGURE 10.** Measured and predicted net loads at Brg 1 & Brg 2 using measured housing vibration as input.[3]

The relative displacement predictions in Figures 8 and 9 correlate very well with the measurements, but the Brg 1 relative displacement is slightly over-predicted by the model and the error is growing roughly linearly with frequency. The authors attribute this primarily to discrepancies between the actual versus measured base motion of Figure 8. This topic is discussed in more depth in [3].

The predicted and measured actuator forces for the two radial bearings are shown in Figure 10. The predicted actuator force is from the system analysis and the measured force is calculated from the measured control current. These forces are "control forces" or the forces produced by the control current in the bearing coils. From Figure 4-6, the combined control force for Brg1 and Brg 2 at 25 Hz is approximately 248 + 348 = 596 lbf. This is considerably higher than the 1.53 G force that might be expected: 1.53*228lbf = 349 lbf total. The discrepancy is due to the "negative stiffness" force pulling the rotor in the opposite direction from the control force such that the net reaction force on the rotor is smaller than the control force. The combined negative stiffness force at 25 Hz for Brg 1 and Brg 2 is approximately (0.0026 + 0.0031) inch * 35,000 lbf/in ~= 200 lbf. Thus the "net reaction force" is 596 – 200 = 396 lbf, very close to what would be expected.

If the magnetic bearings could be made stiff enough such that the rotor motion would closely approximate the housing motion, then the negative stiffness force would be insignificant. In this case, the additional load capacity needed to meet the vibration requirements would simply be the apparent rotor weight associated with the maximum acceleration from Table 1. However, there is a constraint on using a very stiff magnetic bearing as the effect of sensor noise becomes less manageable as compensator gain is increased. Thus, when the housing is being shaken there will be some relative rotor/housing displacement. Even so, the magnetic bearings must be stiff enough such that the relative rotor/housing displacement is less than the backup bearing clearance with some design margin. The penalty associated with maximum expected rotor motion within the actuator must be considered in sizing magnetic bearings (as was done here).

## MIL-S-901D Analysis & Testing

One of the final tests performed on the HESC chiller and compressor was a series of shock tests per MIL-S-901D. The chiller system was mounted via isolation mounts on a barge (the Floating Shock Platform, FSP) which is floated in a large body of water for the test. The shock test entailed subjecting the FSP with operating HESC chiller to a standard sequence of four different shock impacts per Table 2. For Shots 1, 2, and 4 the chiller system was operated at a capacity dictated by reservoir water temperature. The "warm" water input to the chiller during testing was drawn from the reservoir, then cooled by the chiller and discharged back into the reservoir. The shock testing and simulation summarized here was previously covered in more detail by Hawkins.[5]

### Test Conditions

After each test, the system was shut down and the chiller system was inspected for leaks or other damage. Meanwhile, backup bearing clearance checks and magnetic bearing transfer function measurements were performed to verify integrity of these systems. Additional, data collected by the MBC during the test—the fault/event log and high frequency measurements (5 kHz) of sensor position, coil current and commanded current—were reviewed. Following the inspections and data review, the system was returned to operation each time and normal operation was verified. No observable change in backup bearing clearance, backup bearing rolling orbits, or rotor unbalance response were observed after any of the four tests. The closest blast, Shot 4, was the most severe due to the small standoff and the lateral orientation to the main barge axis. The review of test and simulation results below focus on Shot 4.

### Motion Data Collected During Shot 4

Measurements from the shot 4 test are shown in Figs. 11 to 16. Figure 11 shows the vertical, horizontal, and vector magnitude acceleration non-dimensionalized to the peak measured acceleration. This data is from a tri-axial sensor mounted at the

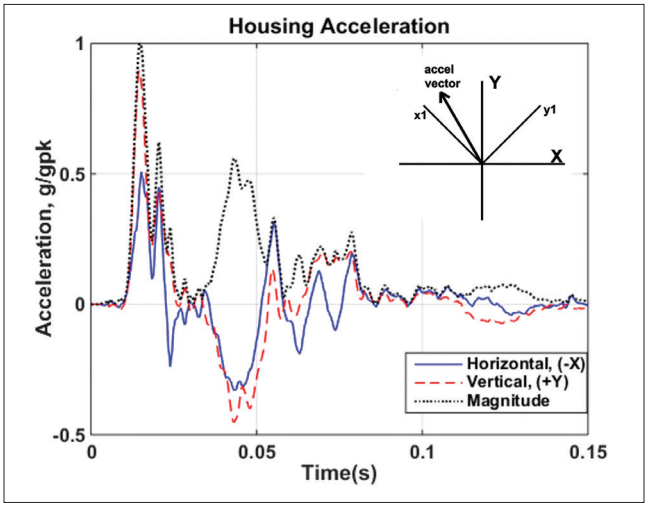


**FIGURE 11.** Measured housing acceleration, g/g_pk.[5]

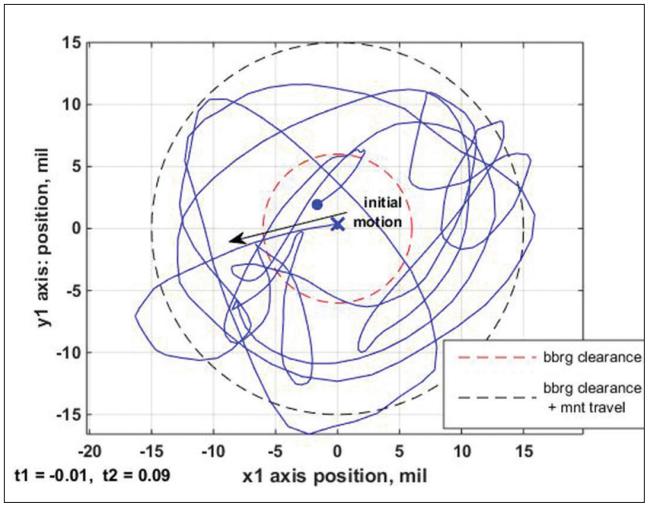


**FIGURE 12.** Shot 4—Shock impact with initial relative rotor/hsg motion measured from Brg 1 pos. sensors.[5]

top of the housing at roughly the axial center of the rotor. The vertical acceleration is higher than horizontal due to the short horizontal standoff of this shot. The peak housing acceleration vector relative to global axes (X,Y) and the magnetic bearing axes (x1, y1 shown) in the inset to Fig. 11. The vertical acceleration can be described as an initial pulse, with each successive half pulse smaller and longer in duration. The complete data set showed another small acceleration peak at about 0.6 seconds (not shown) that is apparently due to the gas bubble from the explosion reaching the surface.

Figures 12 to 15 show a series of 4 orbit plots created from Brg1 position sensor measurements and for successive time periods. On each plot, the earliest point in time is marked by an *x* and the last point in time is marked by a *dot*. The first 0.090 sec of motion following the shock is shown in Figure 12 and includes the three significant half pulses from the acceleration measurement. There are two dashed circles shown on this plot representing: 1) the free backup bearing clearance of 152.4 µm (0.006 in), and 2) the maximum radial rotor housing travel (at the backup bearings) before engaging the hard stop 406.4 µm (0.016 in). The maximum travel includes the free clearance, full deflection of the resilient mount before hard stop, and relative backup bearing inner/outer ring deflection at the load associated with full mount deflection. There are several excursions beyond the hard stop threshold which may be attributable to: 1) the measured position data is from the position sensor axial location and doesn't include additional possible deflection of the rotor between the sensor and backup bearing, and 2) the hard stop is not completely rigid as it has some contact compliance.

From 0.090 sec to 0.240 sec after initiation of the shock, Figure 13, the rotor motion has been attenuated but is still in and out of contact with the backup bearings. The MBC position fault detection scheme has a delay timer that triggers when the rotor position exceeds the fault limit (127 µm/0.005 inch in this case) and trips if the rotor position exceeds the fault limit during a specific portion of the delay period. In this case, the fault trips and de-levitates the rotor 0.250 sec after the delay timer triggers (Figure 14). After delevitation, the rotor executes several forward whirl orbits, and settles to a low frequency rocking motion close to the vertically bottom position in the backup bearings. After the customer defined reset period, with rotor speed greater than 5,000 rpm, the rotor is relevitated in a stable manner as shown in Fig. 15. Following relevitation, the compressor operation continues as designed.

Additional insight into the shock response can be gained by looking at the sensed positions, commanded current and feedback current versus time shown in Figure 16 for the x1 channel. Immediately after the shock impact the bearing hits current limit and the amplifier saturates for a few cycles; this is evidenced by the constant current vs. time slope of the coil current which of course causes the coil current to lag the command. The primary response frequency can be estimated to be about 175 Hz by counting cycles versus time. This approximately coincides with the expected rigid body natural frequency of the rotor mass on the average mount stiffness. Within about 0.060 to 0.070 sec – about the duration of the first three major half pulses of the housing shock response – the amplifier is out of saturation and the bearing is no longer in current limit. At this point, the control is beginning to stabilize the rotor, but the position excursions are still large enough such that the position fault triggers at 0.25 seconds (not shown). A longer fault delay would likely have allowed recovery without trip for this particular shock event.

Following shock testing the backup bearing and resilient mount assembly were removed and inspected. Primary

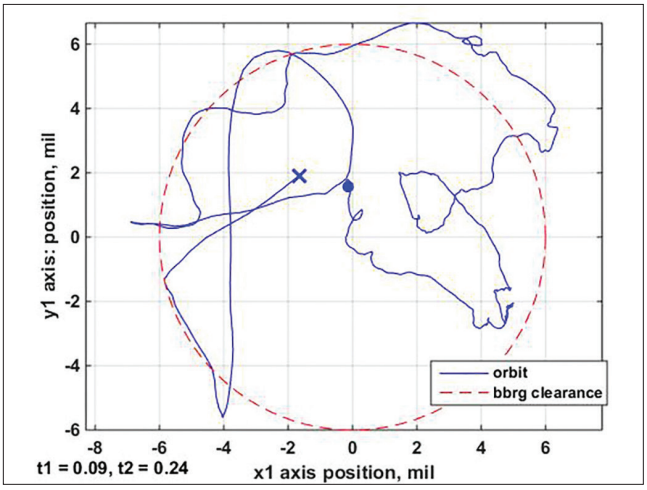


**FIGURE 13.** Shot 4—Rotor bouncing and partial recovery measured from Brg 1 position sensors.[5]

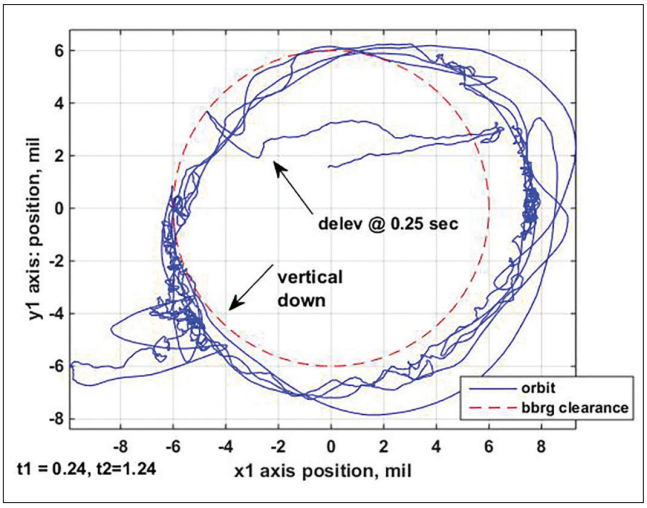


**FIGURE 14.** Shot 4—Drop fault trips 0.250 sec after initial impact and rotor is de-levitated, from Brg 1 sensors.[5]

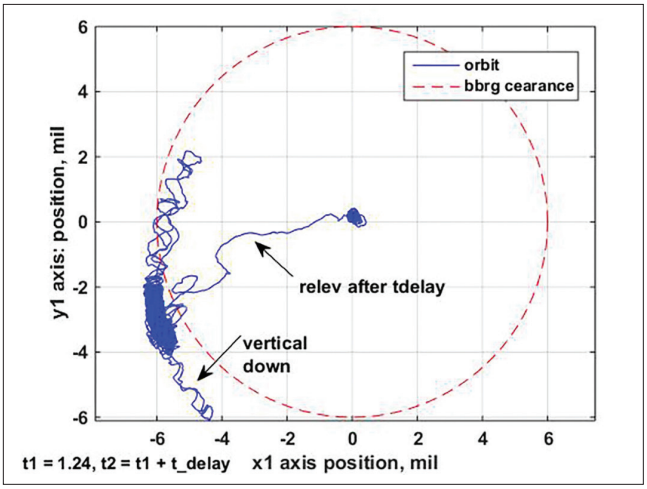


**FIGURE 15.** Shot 4—AutoReset clears fault after t_delay seconds to re-levitate rotor, from Brg 1 sensors.[5]

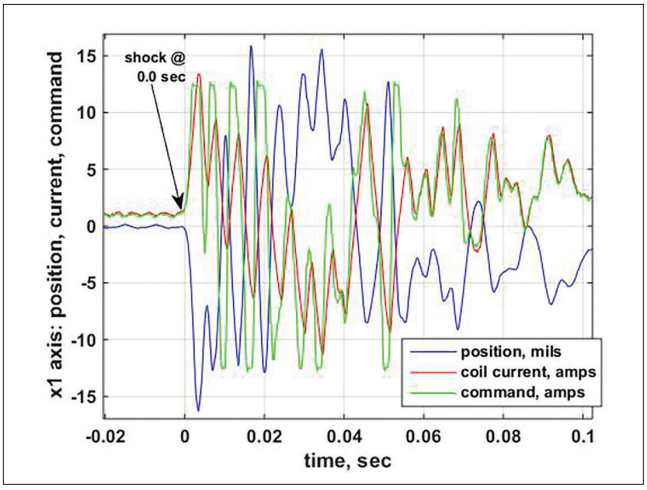


**FIGURE 16.** Measured magnetic bearing reaction to Shot 4, x1 axis: position, commanded current and coil current.[5]

observations were: 1) normal, very light scoring was found on the backup bearing bores and rotor landing surfaces, 2) no evidence found of Brinelling or other raceway defects, and 3) the grease lubrication was intact and appeared normal in color. The backup bearings were reinstalled in the machine and the chiller system was returned to the manufacturers facility where endurance testing was completed without incident. The Navy and chiller manufacturer both concluded that the shock test caused no loss of the designed equipment service life. In contrast the chiller manufacturer typically finds mechanical distress on the load surfaces of oil film bearing supported compressors after shock testing. In this traditional case, some reduction in service life occurs since the shock impact is taken on the *operational bearings* of the compressor.

## Nonlinear, Transient Simulation

Following the shock testing, an existing non-linear simulation tool was used to simulate the shock test using the measured housing acceleration as the driving input. The simulation was used to: 1) understand the reaction of the magnetic bearings and recovery algorithm to the shock event, and 2) predict backup bearing loads during the shock. The simulation involves integration of the system equations of motion (Equation 1 above) using the Newmark-Beta method. The transient and/or nonlinear forces are updated at each integration step and added to the force vector. The linear forces are updated at each integration step—or at a lower rate if so defined—and added to the force vector. Modelling backup bearing clearance, amplitude dependent stiffness, a short term shock input, or magnetic bearing saturation characteristics are straightforward with this approach. An integration time step of 10 μsec was used for the structural dynamic elements.

The magnetic bearing compensator is realized using the same discrete, z domain transfer function coefficients that are used in the MBC digital controller. The magnetic bearing position and current control loops in the simulation are updated at the same rate used in the actual MBC hardware. At each integration time step for the structural dynamic model, the most recent values from each current control loop are multiplied by the appropriate actuator gain (to get force) and added to the force vector.

The key reasons for performing the simulation are to show the response characteristics of the magnetic bearing system – rotor displacements, AMB control, and backup bearing system performance – can be adequately (not perfectly) predicted using housing acceleration as a driving input. This would allow the tool to be used for future risk mitigation, evaluation of design changes, and backup bearing sizing for future machines. Further details on the simulation approach are described in [5].

Figures 17 to 19 show limited results from the Shot 4 shock simulation. Figure 17 shows a displacement orbit plot of the shock impulse and the following 0.09 seconds. The predicted rotor trajectory due to the shock impact is similar to the test data (Fig. 12). The peak predicted excursion is 0.0187, about 5.5% higher than the measured peak of 0.0177 in. The predicted peak response is also sharper than the measured peak response. Several factors may contribute to these differences: 1) the piecewise linear force/deflection curve used for the resilient mount is relatively simple (based on three FEA analysis points, 2) the resilient mount model is axisymmetric whereas the physical hardware is only approximately symmetric, 3) the housing model is rigid whereas the real housing although stiff has some flexibility, and 4) measured housing acceleration is only available for one location on the housing.

Figure 18 shows predicted time history for axis x1 for comparison to the measured data in 16. The amplifier saturation and max current rate correlate well as they should since the hardware characteristics are well defined and easy to model. Also, the response frequency of the first four cycles is 160 Hz, about 10% lower than the measured value (175 Hz). This indicates the effective stiffness of the actual resilient mount over a cycle may be about 20% stiffer than modelled.

Figure 19 shows predicted bearing load for the radial end backup bearing pair around the time of impact. Also shown are the rotor and housing velocities at the associated radial end backup bearing degrees-of-freedom. The load curve is non-dimensionalized by dividing by the load F*

$$\mathbf{F}^* = \ddot{\mathbf{x}}_{\text{cas,pk}}\, \mathbf{m}_{\text{rot}}/2 \qquad (6)$$

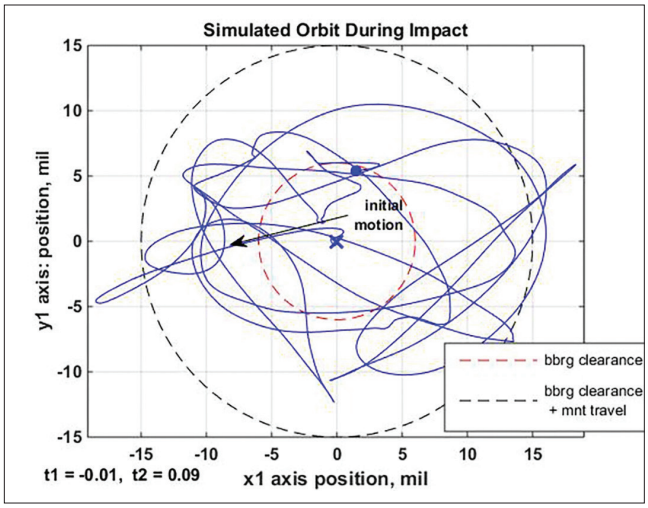


**FIGURE 17.** Shot 4—Predicted Bbrg 1 shock impact with initial relative rotor/hsg motion shown.[5]

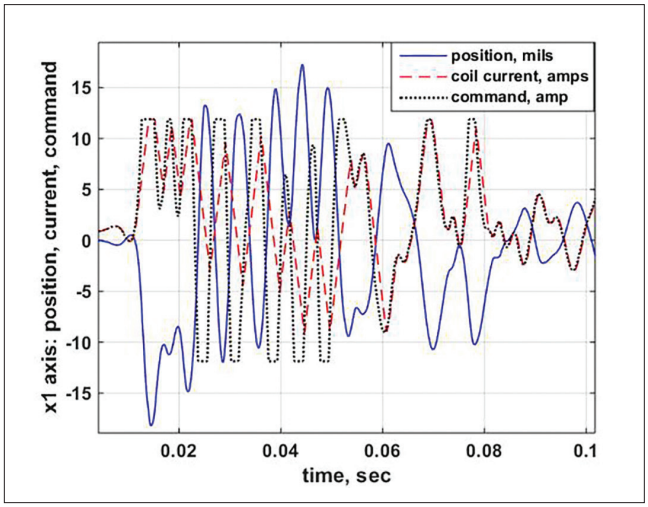


**FIGURE 18.** Shot 4—Predicted magnetic bearing response, x1 axis: position, commanded current and coil current.[5]

where $\boldsymbol{m}_{rot}/2$ is half the rotor mass, and is the peak housing acceleration. The housing acceleration is used because it is generally a design specification or a measured value. The load **F*** is the max load that each backup bearing pair would see if the rotor were accelerated at the peak housing acceleration; the results indicate that the peak rotor acceleration is greater than the peak housing acceleration. This is expected since the housing, together with the backup bearings, impact the stationary rotor with an initial velocity that must be also picked up by the rotor. The velocities are non-dimensionalized by the peak rotor velocity, **V***. The plot clearly shows that the peak bearing loads occur when the rotor and housing velocities are equal, and the rotor velocity is increasing relative to the housing velocity.

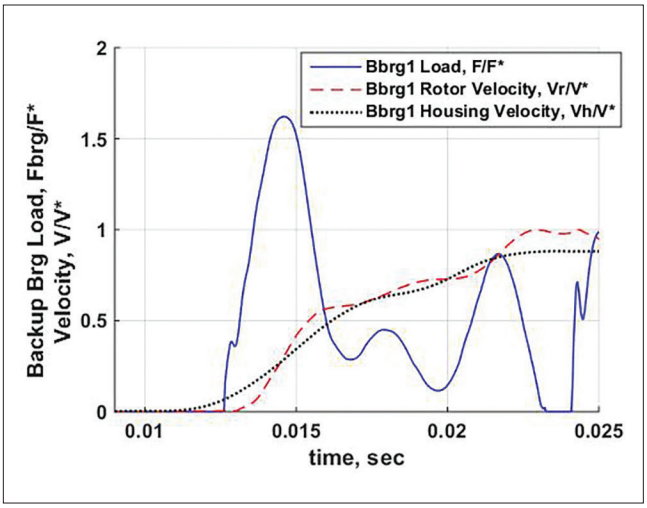


**FIGURE 19.** Shot 4—Predicted backup bearing 1 loads vs. rotor and housing velocity.[5]

## Conclusions

This paper demonstrates the applicability of magnetic bearings and a unique touchdown bearing system to a critical naval application: the HESC chiller system. This application posed unique design challenges related to external vibration and shock requirements. The HESC chiller system adheres to MIL-STD-167-1A, which imposes a vibration response limitation for a spinning, levitated rotor running at full speed and fully loaded. It additionally adheres to MIL-S-901D requirements for external shock loading. A complete analysis was conducted for the machine subject to the criteria in both requirements; these predictions were compared to test measurements for both standards.

For vibration testing, maximum steady-state 0-pk displacement was <0.004", with a backup bearing clearance of 0.006". Maximum steady-state loads were ~350 lbf, approximately half of the radial load capacity. For shock testing, the backup bearing system performed as designed in response to the shock inputs. Peak excursions were well-controlled and the resilient mount provided adequate energy absorption. The shock simulation tool as shown to be suitable for use in future design iterations or new design evaluations.

A complete analysis was conducted for the machine subject to the criteria in both requirements; these predictions were compared to test measurements for both standards. The analyses showed good agreement with the applicable test data. NEJ

## REFERENCES


[1] Naval Sea Systems Command, 2005, MIL-STD-167-1A, *Military Standard, Mechanical Vibrations of Shipboard Equipment,* November

[2] Naval Sea Systems Command, 1989, MIL-S-901D, *Military Specification, Shock Tests, H.I. (High Impact) Shipboard Machinery, Equipment and Systems, Requirements For*, March.

[3] Hawkins, L., Khatri, R., Nambiar, K., 2015, "Test Results and Analytical Predictions for MIL-STD-167 Vibration Testing of a Direct Drive Compressor Supported on Magnetic Bearings", *J. of Engineering for Gas Turbines and Power*, GTP-14-1441, Vol 137, No. 5, May.

[4] Schweitzer, G., Maslen, E.H, 2009, *Magnetic Bearings: Theory, Design, and Application to Rotating Machinery*, Springer Verlag, Berlin, Germany, pp. 288-294.

[5] Hawkins, Wang, Z., Nambiar, K., 2018, "Floating Shock Platform Testing of a Magnetic Bearing Supported Chiller Compressor – Measurements and Simulation Results", GT2018-77031, Presented at ASME Turbo-Expo, June, Oslo, Norway.